ELSEVIER

Nuclear Instruments and Methods in Physics Research A 432 (1999) 111–121

NUCLEAR INSTRUMENTS & METHODS IN PHYSICS RESEARCH Section A

www.elsevier.nl/locate/nima

A feasibility study of boron-loaded liquid scintillator for the detection of electron anti-neutrinos

S.C. Wang[a], C.C. Hsu[b], R.W.S. Leung[a], S.L. Wang[c], C.Y. Chang[a,1], C.P. Chen[a], K.C. Cheng[d], T.I. Ho[c], W.P. Lai[a], H.M. Liu[e], Z.P. Mao[a,2], I.C. Shih[a], H.T. Wong[a,*], Z.Q. Yu[a,2]

[a]*Institute of Physics, Academia Sinica, Nankang, Taipei 11529, Taiwan*
[b]*Department of Physics, National Taiwan University, Taipei, Taiwan*
[c]*Department of Chemistry, National Taiwan University, Taipei, Taiwan*
[d]*Physics Division, Institute of Nuclear Energy Research, Lungtan, Taiwan*
[e]*Nuclear Science and Technology Development Center, National Tsing Hua University, Hsinchu, Taiwan*

Received 20 October 1998; received in revised form 20 March 1999

Abstract

Boron-loaded liquid scintillator offers some potential advantages as a detector for electron anti-neutrinos. A research program was carried out with the objective of developing such scintillators. The crucial feature is the pulse shape discrimination properties following the neutron capture by ^{10}B. Results of the R&D efforts are presented. The feasibility and the technical difficulties of carrying out a full-scale neutrino experiment based on this approach are discussed.

PACS: 14.60.Pq; 19.40.Mc

Keywords: Neutrinos; Liquid scintillator

1. Introduction

Electron anti-neutrinos are abundantly produced at nuclear reactors. Reactor neutrino experiments have been carried out for many years world-wide (For an overview of current status of reactor neutrino experiments, see, for example, Ref. [1]). The central topic in reactor neutrino physics has been the search for neutrino oscillation. Almost all of these experiments made use of the interaction

$$\bar{\nu}_e + p \rightarrow e^+ + n$$

which gives rise to the experimental signatures of a prompt e^+ with two 511 keV γ-rays followed by the delayed capture of the neutron. The correlated signals provide powerful constraints to differentiate the neutrino interactions from the background. A $\bar{\nu}_e$ detector should therefore be rich in proton to provide targets for the $\bar{\nu}_e p$ reactions and also for

*Corresponding author. Tel.: +886-2-2789-9682; fax: +886-2-2788-9828. .
E-mail address: htwong@phys.sinica.edu.tw (H.T. Wong)
[1] Permanent address: University of Maryland, USA.
[2] Permanent address: IHEP, Beijing, China.

0168-9002/99/$ - see front matter
PII: S0168-9002(99)00350-2

neutron thermalization. Accordingly, the experiments [2–8] are all based on liquid scintillator as the detector medium. They differed only in the selected means of neutron capture which is the most important ingredient of the detection. Detection of electron anti-neutrinos is also essential in the studies of neutrinos produced in supernova explosions (see, for example Ref. [9]) or from the Earth's lithosphere (see, for example Ref. [10]).

Liquid scintillators (for a thorough description, see, for example Ref. [11]) have been extensively used as neutron detectors. High-energy neutrons lose their energy primarily through proton recoils in the scintillator which can give rise to light emissions. The total light output due to successive recoil protons is a measure of the energy of the incident neutrons. The thermalized neutrons are then captured with a characteristic delayed time and give rise to certain signatures, producing a tag for the neutron events.

The energy of the $\bar{\nu}_e$ from the $\bar{\nu}_e p$ interactions can be derived from $E_{\bar{\nu}_e} = (E_{e^+} + 1.8)$ MeV where E_{e^+} is the e^+ kinetic energy deposited in the detector medium. The neutrons produced in the $\bar{\nu}_e p$ interactions from reactor, supernova and geo-neutrinos are of lower energy (keV range) and therefore do not contribute to the prompt signals from proton recoils. They will, however, give rise to delayed neutron capture events which provide a characteristic timing signatures for background suppression.

A list of commonly used isotopes for neutron capture is shown in Table 1. They usually have large capture cross sections, high isotopic abundance and give characteristic experimental signatures to differentiate them from the gamma background.

This article describes our efforts to explore the physics case and the technical feasibility of boron-loaded liquid scintillator as an alternative technique to detect electron anti-neutrinos [12]. The motivations, the performance achieved and the technical difficulties encountered are discussed in the subsequent sections.

2. Motivations

If the liquid scintillator is loaded with boron, the emitted neutron will be thermalized in the liquid and then captured by ^{10}B:

$$n + {}^{10}B \rightarrow {}^{7}Li^* + \alpha \ (BR = 94\%;\ Q = 2.3\ MeV)$$

$${}^{7}Li^* \rightarrow {}^{7}Li + \gamma \ (E_\gamma = 480\ keV)$$

or simply

$$n + {}^{10}B \rightarrow {}^{7}Li + \alpha \ (BR = 6\%;\ Q = 2.8\ MeV).$$

The large cross section ($\sigma \sim 4000$ barn) and high isotopic abundance (20%) makes ^{10}B an interesting isotope to provide thermal neutron capture. In particular, liquid scintillator can be produced with a concentration up to the range of 1% ^{10}B by weight (or up to 5% ^{10}B if the isotopic abundance is further enriched), due to the high solubility of

Table 1
Isotopes with good thermal neutron capture cross sections and signatures

Isotope	Natural abundance	Reaction	Cross section (barns)	Signatures
^{3}He	10^{-4}	(n, p)	5.3×10^3	p: 0.574 MeV + ^{3}H: 0.191 MeV
^{6}Li	0.075	(n, α)	9.4×10^2	α: 2.05 MeV + ^{3}H: 2.73 MeV
^{10}B	0.20	(n, α)	3.8×10^3	1.47 MeV α + ^{7}Li: 0.84 MeV + γ: 0.48 MeV
^{113}Cd	0.12	(n, γ)	2×10^4	γ-burst: 8 Mev
^{155}Gd	0.15	(n, γ)	6.1×10^4	γ-burst: 8 Mev
^{157}Gd	0.16	(n, γ)	2.6×10^5	γ-burst: 8 Mev

Table 2
Variation of mean neutron capture time, "straight-line" distance and caputre fraction with ^{10}B concentration, based on an MCNP simulation. The capture time and fraction are independent of the initial neutron energy while an energy of 0.5 keV is used for the capture distance simulation

^{10}B Conc. by weight	Mean capture time (μs)	Mean capture distance (cm)	Capture fraction by ^{10}B
0.0	268	10.9	0.0
0.5	4.7	4.4	0.98
1.0	2.3	4.0	0.99
3.0	0.86	3.1	1.0
5.0	0.62	2.69	1.0
7.0	0.54	2.37	1.0

boron compounds in aromatic solvents. This high concentration leads to a much shorter capture time (a few μs) with $> 99\%$ capture efficiency compared to other good isotopes adopted in other reactor neutrino experiments [2–8] where the capture time is of the range of 30–100 μs: ^{3}He in Goesgen (inhomogeneous detector), ^{6}Li in Bugey (0.1% by weight), and $^{157}Gd + {}^{155}Gd$ in Chooz and Palo Verde (0.1% by weight). The typical capture time in unloaded liquid scintillator is ~ 250 μs. Based on a full neutron transport simulation (MCNP) [13], the variation of mean capture time, "straight-line" distance and capture fraction with ^{10}B concentration is displayed in Table 2. The capture time and fraction is independent of the initial neutron energy, while the capture distance shown is for neutrons with an initial energy of 0.5 keV, a typical range for interactions of $\bar{\nu}_e$ from reactors with protons.

In addition, boron-loaded liquid scintillator has been proposed [14,15] as a solar neutrino experiment, which focuses on both the charged-current and the neutral-current detection:

$$\text{CC: } \nu_e + {}^{11}B \rightarrow e^- + {}^{11}C^*;\ {}^{11}C^* \rightarrow {}^{11}C + \gamma$$

$$\text{NC: } \nu_e + {}^{11}B \rightarrow \nu_e + {}^{11}B^*;\ {}^{11}B^* \rightarrow {}^{11}B + \gamma.$$

Besides neutrino physics, boron-loaded scintillator may also find applications as a cost-effective and efficient large-volume neutron detector system. Boron-loaded liquid [16,17] and plastic [18] scintillators have been studied previously. There exists a commercially available boron-loaded liquid scintillator,[3] but it does not show pulse shape discrimination capabilities on the thermal neutron capture by ^{10}B [19].

3. Experimental details

The setup of our measurement system is shown schematically in Fig. 1. The liquid scintillators were placed in a Pyrex glass cylindrical container, 5 cm in diameter and in length (about 100 cm^3 in volume), which has a high and flat transmittance curve for light of wavelength from 400 to 2000 nm. One of the flat surfaces of the container was coupled via optical grease to a 5 cm diameter photo-multiplier tube (PMT). The remaining surfaces of the Pyrex container were wrapped by aluminum foils as light reflector. The fast PMT[4] has a bialkali photocathode whose spectral response peaks at 420 nm with a 28% quantum efficiency. The anode pulse was fed to a current integrating ADC read out via the CAMAC bus to a personal computer through a GPIB interface. The relative light yield of the various liquid scintillator samples was obtained by comparing the Compton edges created by the 1.33 MeV gamma rays from a ^{60}Co source.

A typical current pulse out of the photomultiplier anode has a rise time of 8 ns and fall time of 20 ns. The pulse shape discrimination (PSD) measurements were done by the "double charge method" [20,21], illustrated in Fig. 1. Three identical anode signals were fanned out. One was connected to a constant fraction discriminator for ADC gate generation (200 ns in width). The other two were delayed with different timing relative to the gate so that the first ADC input was integrated entirely to give the total charge (Q_t) while the second ADC input was integrated partially at the tail to give the partial charge (Q_p). The ratio Q_p/Q_t measures the weight of the tail in the whole pulse and therefore differs for particles with different ionization

[3] Liquid Scintillator BC523A, Bicron, USA.
[4] Hamamatsu model R878.

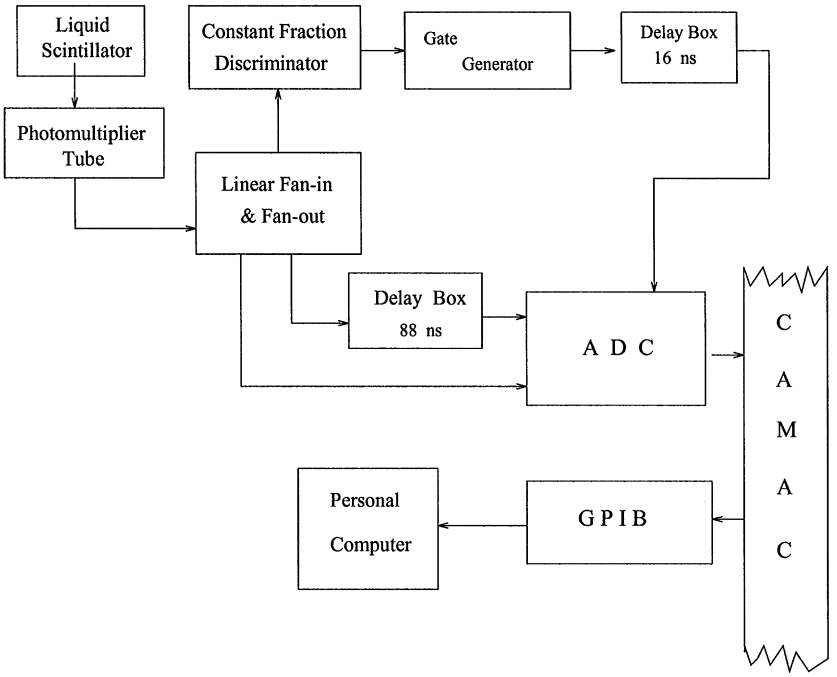

Fig. 1. Schematic layout of the experimental setup.

densities dE/dx. The PSD figure-of-merit, M_{psd}, is defined as

$$M_{psd} = \frac{S_{n\gamma}}{F_n + F_\gamma}$$

where $S_{n\gamma}$ is the separation of the neutron and γ peaks in the Q_p/Q_t spectra, while F_n, F_γ are their full-width at half-maximum.

The attenuation of the liquid scintillator through a 10 cm long cell $A(\lambda)$, in the wavelength range of 300–600 nm was measured by a spectrophotometer.[5] Distilled and de-ionized water in an identical sample holder was used for control measurements. The emission spectra of the liquid scintillator samples $E(\lambda)$ were measured in the same wavelength range by a fluorescence spectrophotometer.[6]

[5] Hitachi U2000.
[6] Hitachi F-3010.

The average bulk attenuation length ($\langle BAL \rangle$) can then be derived by the relation

$$\frac{\sum_i E_i A_i}{\sum_i E_i} = \exp\left[-\frac{x}{\langle BAL \rangle} \right]$$

where $x = 10$ cm is the length of the measuring cell while the summation over i is over the discrete measurements in the wavelength range.

4. Results and discussions

An organic liquid scintillator [11] typically consists of scintillation solutes dissolved in an organic solvent. Charged particles lose their energy through ionization of the solvent molecules. The absorbed energy is transferred to and then excites the solute molecules. The liquid emits fluorescent light as a result of the de-excitation of the solute. A secondary solute of lower concentration is often added to the solution. The purpose is to shift the emission

spectrum of the primary solute towards a longer wavelength for better light transmission through the liquid and matching to the PMT response. The energy resolution and threshold of the scintillator are determined by the number of detected photoelectrons from the PMTs, which depends on the light yield of the liquid.

Different particles (electrons, protons, $\alpha, \ldots$), which have different ionization densities dE/dx, generate pulses of different decay time: the larger the dE/dx, the longer the decaying tail. This allows particle identification through the PSD techniques [16,17,22]. However, high charge densities will lead to reduced light yield or "quenching", due to recombinations and other non-radiative dissipation. Therefore, heavily ionizing particles like α's give much less light than electrons at the same kinetic energy deposited to the liquid scintillator.

Our R&D efforts investigate the handling and performance of boron-loaded liquid scintillator, and in particular, its light yield, attenuation length and PSD properties. The results are discussed below.

4.1. Without boron loading

Both *o*-xylene (C_9H_{10}) and 1,2,4-trimethylbenzene (pseudocumene (PC: C_9H_{12})), at a purity level of 99% ("synthetic grade"), have been used as solvent in the scintillator mixtures. Different solute mixtures were studied. The first one adopted 2,5-diphenyloxazole (PPO: $C_{15}H_{11}NO$) as the primary scintillation solute, whose emission spectrum peaks at around 363 nm, while 1,4-*bis*(2-(5-phenyloxazolyl))-benzene (POPOP: $C_{12}H_{16}N_2O_2$), whose absorption spectrum peaks at 385 nm and emission spectrum at 418 nm, was added as wavelength shifter. The amount of PPO and POPOP was varied and the optimal concentration was determined when the solution gave a maximum light yield. The results are shown in Fig. 2 in the case where *o*-xylene was base solvent. A maximum light yield occurred at a concentration of 4 g/l of PPO plus 50 mg/l of POPOP. However, increasing the solute concentration can deteriorate the light transmission and therefore the compositions of 4 g/l of PPO and 10 mg/l of POPOP were chosen as the starting recipe to optimize other

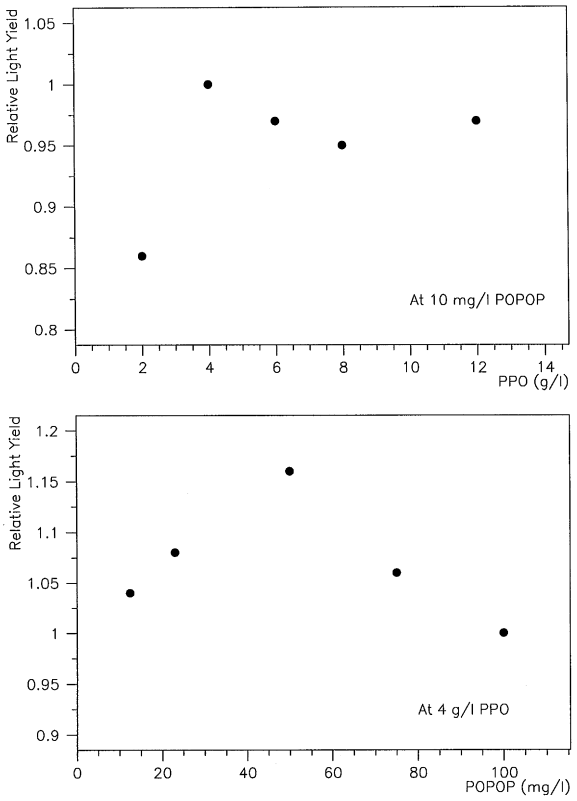

Fig. 2. The variation of the relative light yield with PPO and POPOP concentration, in the case with *o*-xylene as solvent.

properties of the liquid. Other solvents, like PC and mineral oil, at these solute concentrations gave similar light yield results, which were about 65–70% of that from anthracene, a commonly used reference standard.

Emission spectra of different scintillators peaked at around the same wavelength ($\lambda_{peak} \sim 410$–430 nm). Attenuation curves, $L(\lambda)$, however, shifted considerably as the concentrations of solutes changed. Their typical profiles are depicted in Fig. 3 in the case of PC + 4 g/l PPO + 10 mg/l POPOP, where the average attenuation length $\langle BAL \rangle$ was 6.5 m.

Another scheme involved using 1-phenyl-3-mesityl-2-pyrazoline (PMP) as a single solute in the liquid scintillator, to benefit from its large Stokes shift (absorption peaks at 295 nm; emission peaks at 425 nm). The light yield was comparable with that of PPO + POPOP.

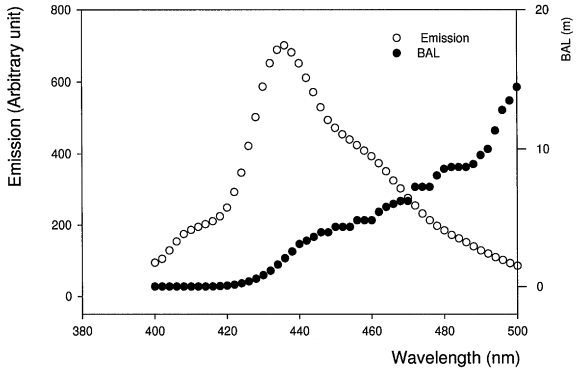

Fig. 3. The emission spectra and the bulk attenuation length for the PC + PPO + POPOP scintillator.

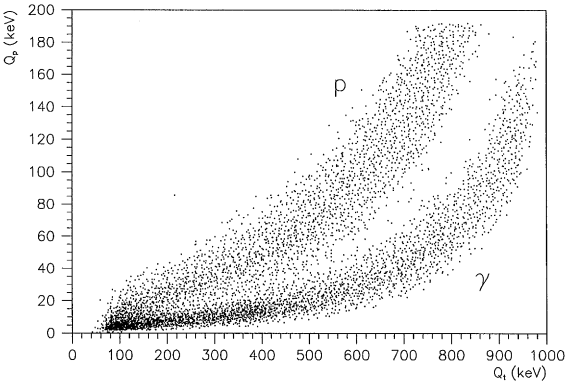

Fig. 4. The scattered plot of Q_p versus Q_t from a PC + PPO + POPOP solution due to a neutron source, showing different response to γ and proton recoils at energy above 200 keV.

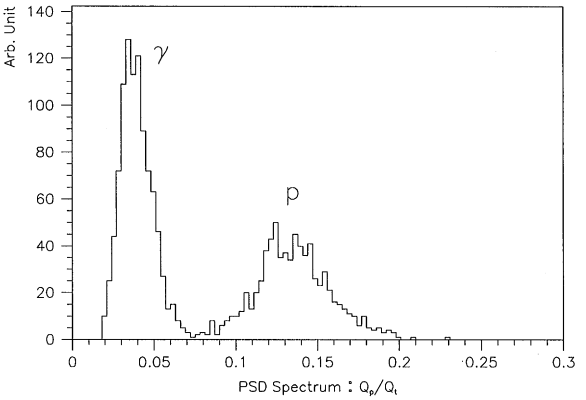

Fig. 5. The PSD spectrum of the PC + PPO + POPOP solution at the 500 keV energy bin.

To study the PSD properties of the scintillator at the >200 keV electron-equivalence energy range, the proton recoil signatures due to a ^{241}Am/Be neutron source (neutron energy of 4–8 MeV) were measured. Energy calibration was done using the Compton edges of the 0.66 keV and 1.33 MeV γ-rays from the ^{137}Cs and ^{60}Co sources, respectively. A typical Q_p versus Q_t scattered plot and the "PSD spectrum" (Q_p/Q_t ratio) for the PC + 4 g/l PPO + 10 mg/l POPOP solution are depicted in Figs. 4 and 5, respectively. Alternatively, PSD was also observed with a solution of ^{241}Am source dissolved into the scintillator. The emitted 5.4 MeV α's gave an electron-equivalence light yield of 430 keV. The reduction of light was due to the quenching effects as discussed.

The PSD property of a scintillator improves as the amount of slow components (like PMP and naphthalene (NPT: $C_{10}H_8$)) increases in the solution. However, self absorption of scintillation in the solution also increases with the amount of solutes. As an illustration, the PSD figure of merit using the ^{241}Am α-source and the average BAL as a function of NPT concentration in a PC + 4 g/l PPO + 10 mg/l POPOP solution is shown in Fig. 6. Therefore, depending on application, an optimization has to be made between PSD and bulk attenuation length.

The choice of solvents may also affect the PSD properties. Mineral oil tends to degrade PSD while *o*-xylene and PC are compatible. The degradation of M_{psd} as a function of mineral oil concentration in a PC + PPO + POPOP solution is shown in Fig. 7.

4.2. With boron loading

Boron was dissolved in the liquid scintillator samples via the solution trimethylborate (TMB: $(CH_3)_3BO_3$), which contains 10.3% of boron by weight. Scintillator mixtures with TMB concentration as high as 80% have been prepared giving an 8% boron content by weight. Even with the natural

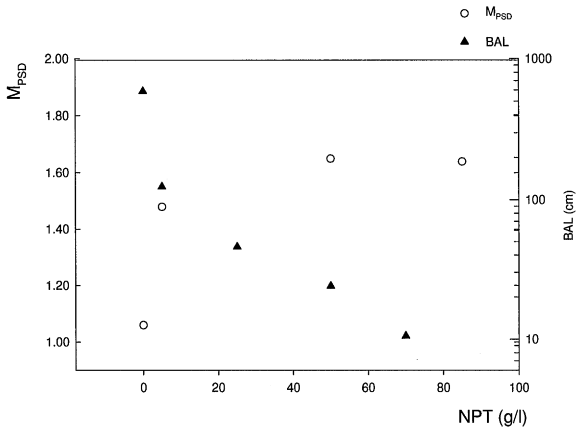

Fig. 6. The variation of PSD performance and average bulk attenuation length with NPT concentration.

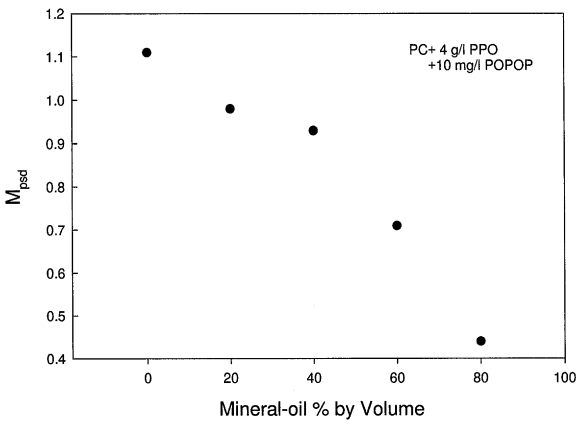

Fig. 7. The variation of PSD performance with mineral oil concentration in a PC + PPO + POPOP solution.

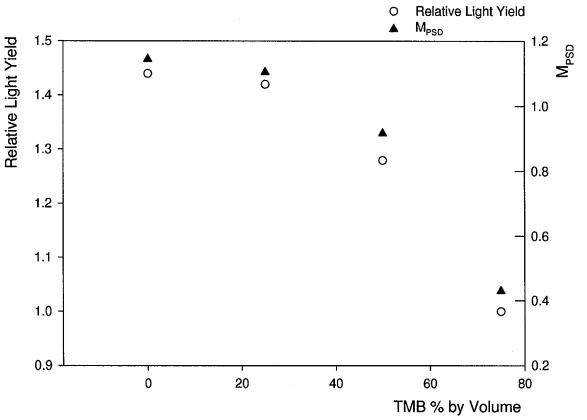

Fig. 8. The variation of relative light yield and PSD performance with TMB concentration in a PC + 4 g/l PPO + 10 mg/l POPOP solution.

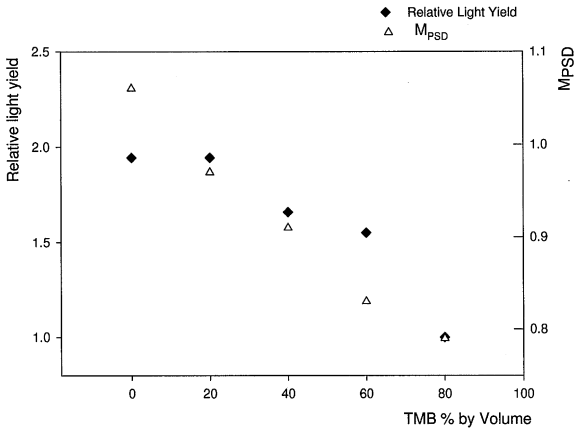

Fig. 9. The variation of relative light yield and PSD performance with TMB concentration in a PC + 10 g/l PMP solution.

isotopic abundance of 19.8% for ^{10}B, solutions with ^{10}B as high as 1.6% can be produced. This contrasts with the lithium- and gadolinium-loaded liquid scintillators where the loading is typically only 0.1%. This will greatly reduce the thermal neutron capture time, as shown in Table 2.

The measured effects in the light yield and PSD performance due to a varying TMB concentration are displaced in Figs. 8 and 9, for the cases of PC + 4 g/l PPO + 10 mg/l POPOP, PC + 10 g/l PMP, respectively. If TMB is a completely passive spectator in the scintillating process, one would expect a drop in the light yield proportional to the decrease in the amount of the solvent (in this case PC). However, measurements showed that the light yield dropped by only 20% with TMB being 50% by volume (that is, PC concentration reduced by 50%). The results indicated that TMB took the role as part of solvent in the solution. The PSD performance was also affected by increasing the TMB concentration, due to the reduction in light yield.

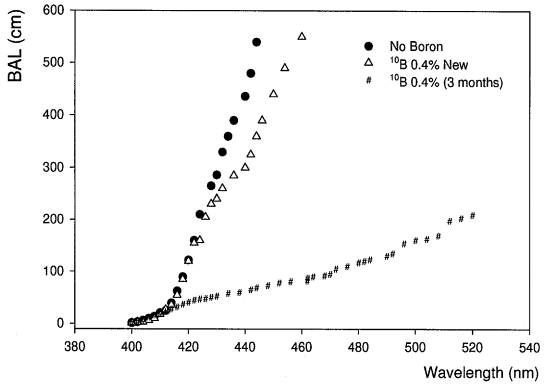

Fig. 10. The BAL variation with wavelength for the PC + PPO + POPOP + TMB mixture, showing deterioration of light transmission with time.

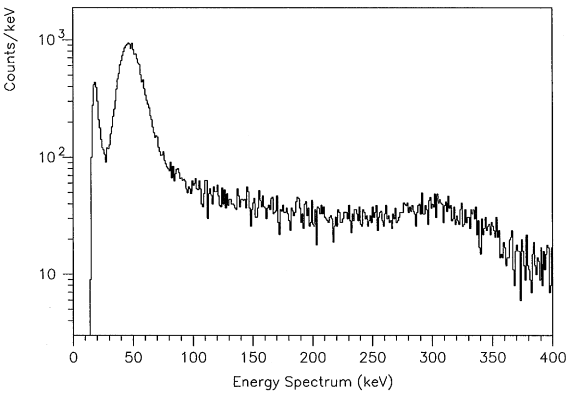

Fig. 11. Energy spectrum measured with the PC + PPO + POPOP + DPA + TMB solution exposed to a neutron source. The peak at 50 keV comes from neutron capture by ^{10}B while the Compton edge is due to the 480 keV γ from the ^{7}Li* final state.

When the TMB-loaded liquid scintillator was freshly and cleanly prepared, the light transmission was only slightly affected. However, there was obvious degradation after the solution was left in a sealed contained for three months, as depicted in Fig. 10.

The principal reason of loading boron to the scintillator is to detect the thermal neutron capture. This process was studied with the ^{241}Am/Be neutron source. The neutrons emitted at 4–8 MeV were moderated by paraffins and water before getting into the detector. The typical thermal neutron capture energy spectrum for the boron-loaded scintillators prepared is shown in Fig. 11. The capture products (BR 94%) of α at 1.47 MeV and ^{7}Li* at 0.84 MeV energy gave rise to only about 50 keV of electron-equivalence energy. Calibration at this energy range was achieved by the 60 keV X-rays from a ^{241}Am source. This result is consistent with those from previous measurements [16,17,19]. The reduction in light yield was therefore more significant than in the case of the 5.4 MeV α's from a ^{241}Am source (where the electron-equivalence light yield was about 430 keV). This is due to the fact that ionization density dE/dx is enhanced for lower kinetic energy making the quenching more severe. The edge at 350 keV in the spectrum was from the Compton edge of the 480 keV γ-rays associated with the de-excitation of the ^{7}Li* plus the α-peak energy.

Table 3
Comparison between the commercially available boron-loaded liquid scintillator with the one developed in this work, based on a PC + PPO + POPOP + TMB mixture

	Commercial[a]	This work
Mean attenuation length	4m	3.2 m
Relative light yield	1.00	0.96
PSD figure of merit[b]	0.9	0.92
% ^{10}B by weight	4.4% (90% enriched)	1.0% (natural)

[a] Liquid scintillator BC523A, Bicron, USA.
[b] At 500 keV electron-equivalence of energy.

As summarized in Table 3, the PC + POP + POPOP + TMB liquid scintillator prepared has comparable performance as the commercial scintillator (see footnote 3). The cost is much reduced, an essential requirement for developing large system. However, both of them do not exhibit PSD capabilities to differentiate neutron capture events from background γs at this low light yield.

To achieve low-energy PSD [16,17], a solute with long decay time constant (9 ns as compared to the 1–2 ns for other solutes), 9,10-diphenylanthracene (DPA: $C_{26}H_{18}$) was added to the solution. Displayed in Fig. 12 is the plot of Q_p versus Q_t with

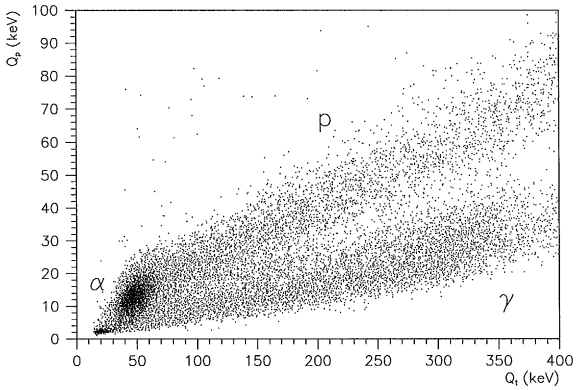

Fig. 12. The scattered plot of Q_p versus Q_t from a PC + PPO + POPOP + DPA + TMB solution exposed to neutron source, showing different response to γ, α and protons.

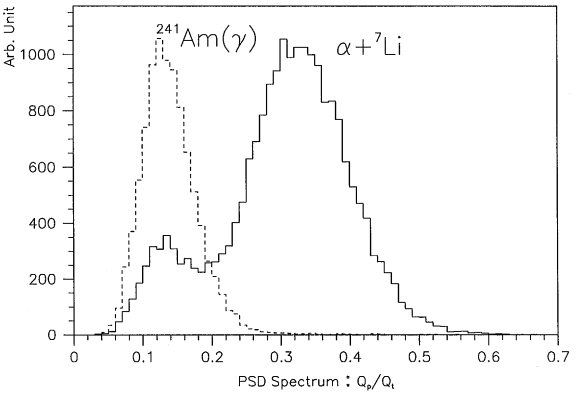

Fig. 13. Measured PSD spectrum of the PC + PPO + POPOP + DPA liquid scintillator loaded with 1.0% ^{10}B by weight: γ from ^{241}Am (60 keV) and α + ^{7} Li from the neutron capture of ^{10}B (50 keV).

the ^{241}Am/Be neutron source and liquid scintillator mixture with 10 g/l of DPA. Two bands corresponding to proton and electron recoils can be seen at high energy. The big blob at 50 keV energy corresponded to the α + ^{7}Li* from the neutron capture events. There was a change of slope between the low- and high-energy portion of the upper band because they were due to different processes: neutron capture and proton recoil, respectively. The M_{psd} spectrum at the capture energy is shown in Fig. 13, where $M_{psd} = 0.8$. The γ peak was due to the 60 keV X-rays from the ^{241}Am source.

The effects on the performance parameters, due to variation in DPA concentration were studied and the results are displayed in Fig. 14. The relative light yield and PSD performance at the neutron capture energy range were measured with the PC + PPO + POPOP scintillator solution mixed with 50% TMB by volume (corresponding to about 1% ^{10}B by weight). The average BAL was obtained with the PC + PPO + POPOP solution without TMB, to decouple the unstable effects of TMB in the light transmission. It can be seen that there is substantial improvements in PSD as DPA concentration increases. The γ and α + ^{7}Li* peaks in the PSD-spectra became distinguishable when DPA concentrations were above 3 g/l (which gave $M_{psd} > 0.3$). Light yield was reduced only slightly.

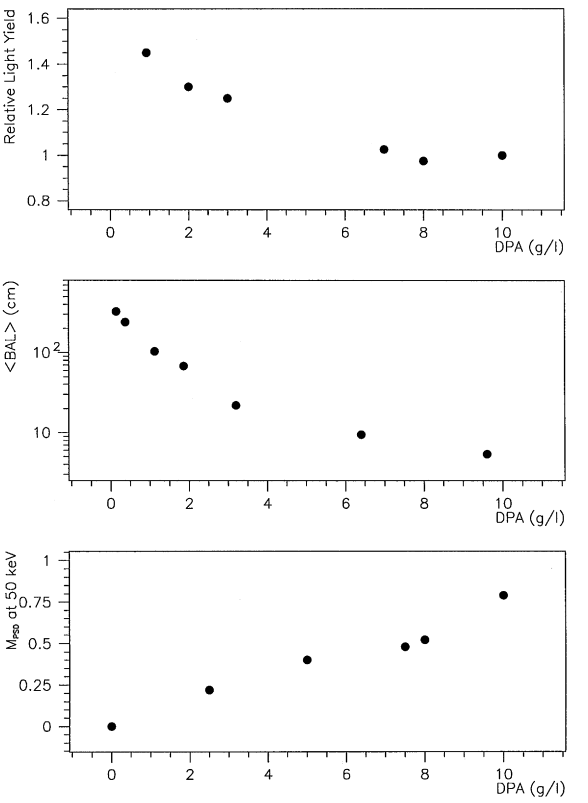

Fig. 14. The variation of relative light yield, average bulk attenuation length and PSD performance with DPA concentration, in the PC + PPO + POPOP + TMB solution.

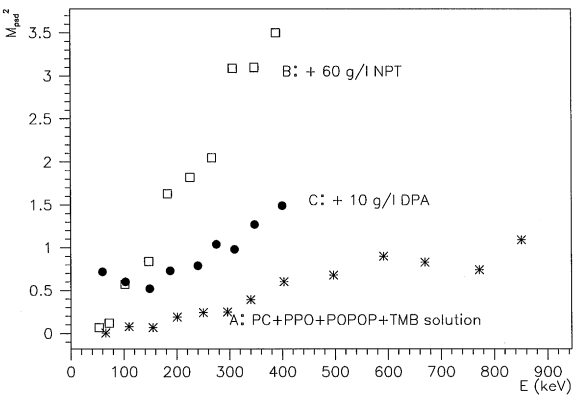

Fig. 15. The variation of PSD performance, in terms of M_{psd}^2, as a function of energy for the (A) PC + PPO + POPOP + TMB, (B) + NPT and (C) + DPA scintillator solutions.

However, the enhancement in PSD was at the expense of light transmission. The $\langle$BAL$\rangle$ dropped below 1 m for DPA concentrations above 1 g/l. The short BAL was due to strong absorptions of DPA at wavelength below 420 nm, while the emission peak of the liquid was only at 436 nm and hence greatly affected by the tails of the absorption spectra.

The PSD performance of various liquid scintillator mixtures over a wide energy range using the ^{241}Am/Be neutron source has been studied. The results are depicted in Fig. 15 for the PC + 4 g/l PPO + 10 mg/l POPOP + 50% TMB solution, as well as for those with additions of 60 g/l NPT or 10 g/l DPA. It can be seen that M_{psd}^2 is proportional to the energy (that is, PSD $\propto \sqrt{\text{No. p-1hotoelectrons}}$), with the proportional constant depending on the solutes in the liquid. Solutions with DPA give the best PSD at low energies (the neutron capture range of 50 keV), while those with NPT enhance the PSD capabilities at higher energy.

5. Feasibility for large-scale detector systems

The results presented above indicate that large-scale (tons in mass or meters in dimension) deployment of a boron-loaded liquid scintillator is possible if one does not require PSD capabilities for the neutron capture events. Using the scintillators described in Table 3, high-energy neutrons can slow down via proton recoils which give PSD signatures, and within a delay time scale of less than 5 μs, will be captured generating an event with 50 keV electron-equivalence energy which does not have PSD information.

However, for applications where PSD tags for the neutron capture events are necessary, there are several hurdles making a large detector system based on boron-loaded liquid scintillator difficult and impractical.

1. The "electron-equivalence" energy of the neutron capture by ^{10}B is only about 50 keV, as depicted in Fig. 11. The PSD at such a low light yield is extremely difficult, and requires additions of DPA which degrades light transmission. A different solute which has comparable long decay-time constant as DPA but with less severe absorption at 420 nm has to be identified. The background at this low energy – and the typical X-ray range – is also a major concern.
2. The chemical TMB is extremely hygroscopic. On exposure to air, it turns into boric acid (a white powder) immediately, via the reaction

$$(CH_3)BO_3 + 3H_2O \rightarrow B\,(OH)_3 + 3CH_3OH$$

which severely affects the light transmission. Placing in an open container in the laboratory, the attenuation length of the TMB-loaded scintillator degrades from meters to centi-meters in the time-scale of minutes. Elaborate purification and circulation systems have to be constructed for large-volume applications.
3. The neutron capture by ^{10}B is accompanied by the emission of a 480 keV γ-ray with a branching ratio of 94%. This photon, if it re-interacts at the same cell as the neutron capture, will severely affect the PSD capabilities, especially so when the electron-equivalence light yield for the $\alpha + {}^7$Li system is only about 50 keV. This effect was studied with a full simulation and the results are displayed in Fig. 16, which shows the probability of the 480 keV γ giving more than 50 keV of energy within the same circular cell as a function of cell radius. It can be seen that the contamination is as high as 60% for a cell radius of 10 cm.

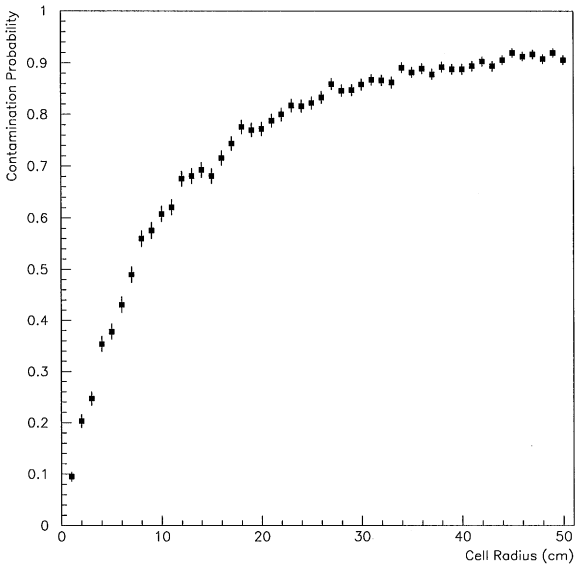

Fig. 16. Simulated contamination probability from the 480 keV γ-rays, as a function of radius for a long cylindrical detector with length much larger than its diameter.

6. Conclusion

Boron-loaded liquid scintillator may have some attractive features as an electron anti-neutrino detector. The concentration of ^{10}B can be much higher than other good neutron capture isotopes. The feasibility of realizing a large-scale detector system based on this technique was explored. A scintillator which can be used in large system and with comparable performance as a commercial one was developed. Both scintillators give electron-equivalence light yield of about 50 keV for neutron capture events, but do not show PSD signatures at this low energy. PSD for such events was realized with the addition of the solute 9,10-diphenylanthracene, but at the expense of greatly deteriorating the light transmission. Several technical hurdles have to be overcome before such an approach can be adopted in a large-scale detector system which requires PSD capabilities for the neutron capture events.

Acknowledgements

The authors would like to thank the technical staff of our institutes for the many contributions. This work was supported by grant NSC 86-2811-M-001R from the National Science Council, Taiwan.

References

[1] Y. Suzuki (Ed.), Neutrino '98 Proceedings; Nucl. Phys. B (Proc. Suppl.) (1998), in press.
[2] G. Zacek et al. (Gösgen), Phys. Rev. D 34 (1986) 2621.
[3] A.I. Afonin et al. (Rovno), Sov. Phys. JETP 67 (2) (1988) 213.
[4] G.S. Vidyakin et al. (Krasnoyarsk), JETP Lett. 59 (1994) 364.
[5] B. Achkar et al. (Bugey), Nucl. Phys. B 434 (1995) 503.
[6] Z.D. Greenwood et al. (Savannah River), Phys. Rev. D 53 (1996) 6054.
[7] M. Apollonio et al. (Chooz) Phys. Lett. B 420 (1998) 397.
[8] F. Boehm et al. (Palo Verde), Palo Verde Proposal, 1993.
[9] D. Kielczewska, Int. J. Mod. Phys. D 3 (1994) 331.
[10] L.M. Krauss, S.L. Glashow, D.N. Schramm, Nature 310 (1984) 191.
[11] J.B. Birks, Theory and Practice of Scintillation Counting, Pergamon, New York, 1964.
[12] C.Y. Chang, S.C. Lee, H.T. Wong, Nucl. Phys. B 66 (Proc. Suppl.) (1998) 419.
[13] J.F. Briesmeister (Ed.), MCNP – A General Monte Carlo N-particle Transport Code, Version 4A, LA-12625-M, 1993.
[14] R.S. Raghavan, S. Pakvasa, Phys. Rev. D 37 (1988) 849.
[15] G. Ranucci, Borex Collaboration, Nucl. Instr. and Meth. A 315 (1992) 229.
[16] H.E. Jackson, G.E. Thomas, Rev. Sci. Instrum. 36 (1965) 419.
[17] L.R. Greenwood, N.R. Chellew, Rev. Sci. Instrum. 50 (4) (1979) 466.
[18] D.M. Drake, W.C. Feldman, C. Hurlbut, Nucl. Instr. and Meth. A 247 (1986) 576.
[19] T. Aoyama et al., Nucl. Instr. and Meth. A 333 (1993) 492.
[20] C.L. Morris et al., Nucl. Instr. and Meth. 137 (1976) 397.
[21] M.S. Zucker, N. Tsoupas, Nucl. Instr. and Meth. A 299 (1990) 281.
[22] R.A. Winyard, J.E. Lutkin, G.W. McBeth, Nucl. Instr. and Meth. 95 (1971) 141.